Supplementary Information for Cecilia et al. It's risky to wander in September: modelling the epidemic potential of Rift valley fever in a Sahelian setting

Contents

1 The model

1.1 Equations

$$
\begin{cases}
\text{Vector population: } \textit{Aedes vexans arabiensis} \text{ (Ferlo) or } \textit{Culex tritaeniorhynchus} \text{ (SRDV)} \\
\frac{dS_1}{dt} = b_1 N_1 - d_1 S_1 - a_1 \phi_{12} \frac{I_2}{N_2} \alpha_{21} S_1 - a_1 \phi_{13} \frac{I_3}{N_3} \alpha_{31} S_1 \\
\frac{dE_1}{dt} = -d_1 E_1 + a_1 \phi_{12} \frac{I_2}{N_2} \alpha_{21} S_1 + a_1 \phi_{13} \frac{I_3}{N_3} \alpha_{31} S_1 - \epsilon_1 E_1 \\
\frac{dI_1}{dt} = \epsilon_1 E_1 - d_1 I_1 \\
N_1 = S_1 + E_1 + I_1 \\
\\
\text{Host population: Cattle} \\
\frac{dS_2}{dt} = b_2 N_2 - d_2 S_2 - a_1 \phi_{12} \frac{I_1}{N_2} \alpha_{12} S_2 - a_4 \phi_{42} \frac{I_4}{N_2} \alpha_{42} S_2 \\
\frac{dE_2}{dt} = -d_2 E_2 + a_1 \phi_{12} \frac{I_1}{N_2} \alpha_{12} S_2 + a_4 \phi_{42} \frac{I_4}{N_2} \alpha_{42} S_2 - \epsilon_2 E_2 \\
\frac{dI_2}{dt} = -d_2 I_2 + \epsilon_2 E_2 - \gamma_2 I_2 - \mu_2 I_2 \\
\frac{dR_2}{dt} = -d_2 R_2 + \gamma_2 I_2 \\
N_2 = S_2 + E_2 + I_2 + R_2 \\
\\
\text{Host population: Small ruminants} \\
\frac{dS_3}{dt} = b_3 N_3 - d_3 S_3 - a_1 \phi_{13} \frac{I_1}{N_3} \alpha_{13} S_3 - a_4 \phi_{43} \frac{I_4}{N_3} \alpha_{43} S_3 \\
\frac{dE_3}{dt} = -d_3 E_3 + a_1 \phi_{13} \frac{I_1}{N_3} \alpha_{13} S_3 + a_4 \phi_{43} \frac{I_4}{N_3} \alpha_{43} S_3 - \epsilon_3 E_3 \\
\frac{dI_3}{dt} = -d_3 I_3 + \epsilon_3 E_3 - \gamma_3 I_3 - \mu_3 I_3 \\
\frac{dR_3}{dt} = -d_3 R_3 + \gamma_3 I_3 \\
N_3 = S_3 + E_3 + I_3 + R_3 \\
\\
\text{Vector population: } \textit{Culex poicilipes} \\
\frac{dS_4}{dt} = b_4 N_4 - d_4 S_4 - a_4 \phi_{42} \frac{I_2}{N_2} \alpha_{24} S_4 - a_4 \phi_{43} \frac{I_3}{N_3} \alpha_{34} S_4 \\
\frac{dE_4}{dt} = -d_4 E_4 + a_4 \phi_{42} \frac{I_2}{N_2} \alpha_{24} S_4 + a_4 \phi_{43} \frac{I_3}{N_3} \alpha_{34} S_4 - \epsilon_4 E_4 \\
\frac{dI_4}{dt} = \epsilon_4 E_4 - d_4 I_4 \\
N_4 = S_4 + E_4 + I_4
\end{cases}
\tag{S.1}
$$

$$
a_i = \frac{1 + c_i}{g_i(T)} \; i \in \{1, 4\} \tag{S.2}
$$

a_i: biting rate of vector population i.
$g_i(T)$: lenght of the gonotrophic cycle, function of temperature T, of vector population i.
c_i: proportion of double blood meals; $1 + c_i$ therefore being the feeding rate per gonotrophic cycle of vector population i.

$$
\phi_{ij} = \frac{\pi_{ij} N_j}{\pi_{i2} N_2 + \pi_{i3} N_3} \; i \in \{1, 4\}, j \in \{2, 3\} \tag{S.3}
$$

For each vector population i, $\pi_{i2} + \pi_{i3} = 1$.

1.2 Parameterization

Inclusion of input data from previous models

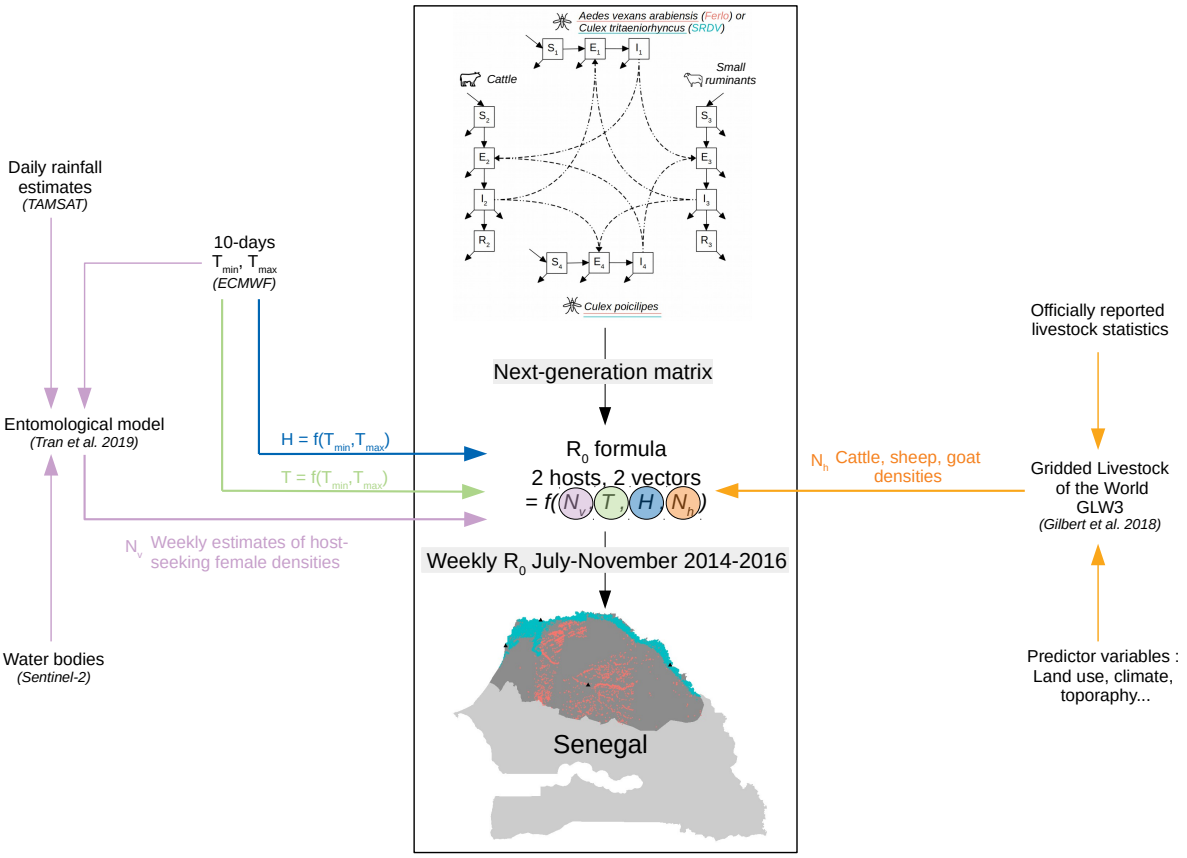

Figure S.1: Modelling framework of the study. We built a mechanistic model of Rift Valley fever virus transmission with 2 host and 2 vector populations in two study areas belonging to different ecosystems (Ferlo and Senegal river delta and valley, SRDV). We derived the basic reproduction number R_0 using the next generation matrix approach (see Supplementary Information 2, Eq 1-5 in main text). We then used input data from various sources to compute R_0 for weekly introduction dates, for each pixel containing both hosts and vectors, for three consecutive rainy seasons (July-November 2014, 2015, and 2016) in northern Senegal.

$H = 100.\frac{exp(\frac{17.27(T_{min}-2)}{(T_{min}-2)+237.3})}{exp(\frac{17.27T_{max}}{T_{max}+237.3})}$, $T = (T_{min} + T_{max})/2$. TAMSAT : Tropical Applications of Meteorology using SATellite. ECMWF: European Center for Medium Range Weather Forecasts.

Minimum and maximum temperatures over 10-day periods, T_{min}, T_{max} were retrieved from the European Centre for Medium Range Weather Forecasts (ECMWF). These temperatures were used to compute the relative humidity H as follows:

$$H = 100.\frac{exp(\frac{17.27(T_{min}-2)}{(T_{min}-2)+237.3})}{exp(\frac{17.27T_{max}}{T_{max}+237.3})} \tag{S.4}$$

The relative humidity was then used to compute mortality rates of *Culex* populations (see Table 1 in main text). Temperature-dependent functions related to vector parameters (mortality rate, biting rate and extrinsic incubation period, see Table 1 in main text) were computed with:

$$T = (T_{min} + T_{max})/2 \tag{S.5}$$

Temperature variations in the study area were not wide (Figure S.2). In addition, we can notice that a given temperature distribution is not a good predictor of the epidemic potential at the regional scale (similar distributions induce different pxl_1).

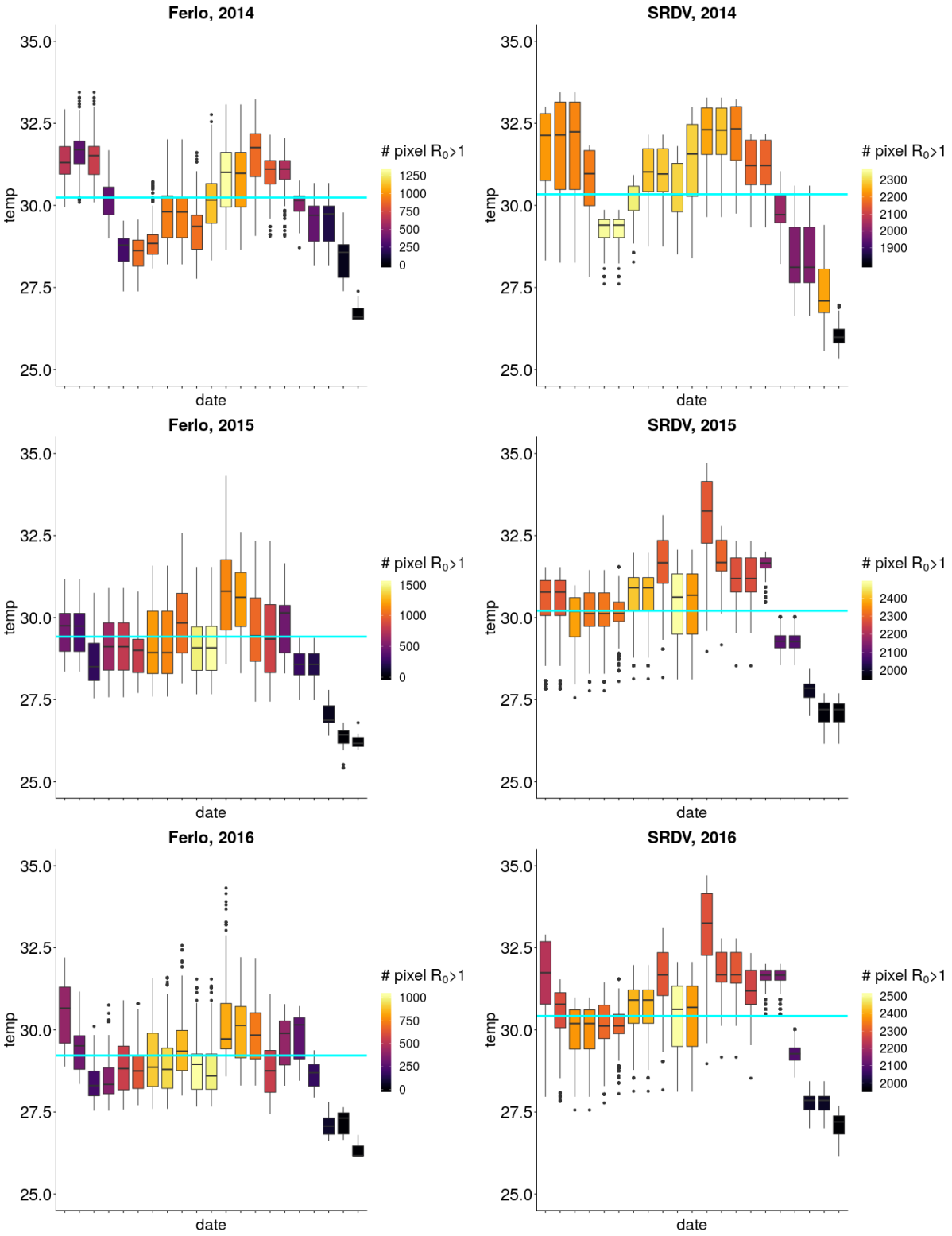

Figure S.2: Temperature distribution by virus introduction date for each rainy season, spatially aggregated by study area (left : Ferlo, right : SRDV). Boxplots are coloured by the number of pixels with $R_0 > 1$ (pxl_1) for a given study area and introduction date. The blue line indicates the mean temperature over the rainy season.

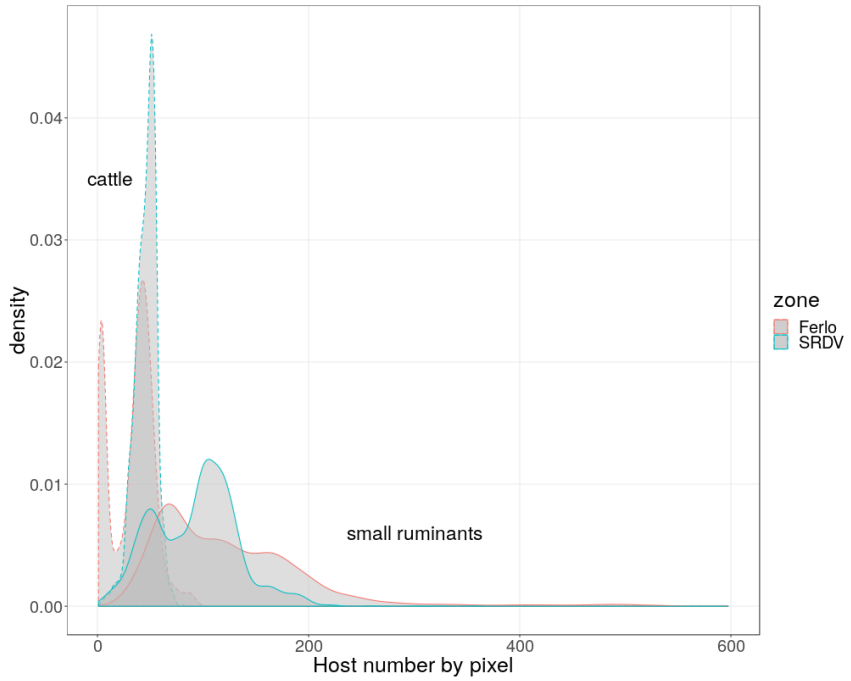

Figure S.3: Distribution of host densities within pixels, by population and study area. Dashed lines are for cattle, solid lines for small ruminants. Red lines for Ferlo, blue ones for SRDV.

Vector parameters

- Gonotrophic cycle : this cycle consists in searching for a vertebrate host, blood feeding, blood meal digestion, egg maturation and oviposition. Mating only happens once for females. Here we used the ovarian development time as a proxy, which is the longest part of the gonotrophic cycle and is temperature-dependent. We used the same equation for every vector population, taken from Madder et al. 1983 for *Culex pipiens* in field conditions. Values are consistent with what was measured by Ndiaye et al. 2006 on *Ae. v. arabiensis* collected in Barkedji.

- Multiple blood meals : It is generally assumed that one blood meal takes place by gonotrophic cycle, but there are conditions where mosquitoes have to take multiple partial blood meals, because of host defense mechanisms for instance. This changes the contact rate between vectors and hosts and influences disease transmission. We decided to include it in our study, as it has been evidenced in several species in non-trivial proportions.
  Ba et al. 2006 showed 16.88% (n=693) of multiple blood meals in naturally fed *Aedes vexans* in the Ferlo region. Edman and Downe 1964 showed 18.5% (n=1417) of multiple blood meals for *Aedes vexans* in Kansas, USA.
  Multiple blood meals have also been evidenced in *C. poicilipes* in Muturi et al. 2008 (Kenya, 73.3%, n=11), Gordon et al. 1991 (Senegal, 2.2%, n=91) and Crabtree et al. 2013 (Uganda, 0.4%, n=40). These studies were sometimes able to detect more than two different origins in the blood meals, but we decided to limit our model complexity and consider these proportions as double bites only. We favoured values from studies on *Aedes vexans* because of their bigger sample sizes. We chose 17% as reference value, which was consistent with the two studies at our disposal, and applied it to every vector population. We considered *C. tritaeniorhynchus* to exhibit the same kind of behaviour.

- Extrinsic incubation period : We used an equation calibrated by Barker et al. 2013 including data from a study conducted on *Aedes fowleri* in Senegal (Turell 1989). We applied it to every vector population.

Host parameters

- Density downscaling : Gridded Livestock of the World (GLW3, Gilbert et al. 2018) pixel resolution is 100km^2. Tran et al. 2019 pixels are hexagons of 1km radius, which corresponds to $\frac{6}{\sqrt{(3)}} km^2$.
  GLW3 animal densities were therefore divided by $\frac{100 \times \sqrt{(3)}}{6}$ and assigned to Tran et al. 2019 pixel centroids.

- Lifespan : Based on expert opinion, cattle (mostly Gobra Zebu) live 8 years on average in our study region. For small ruminants, Table S2 of Hammami et al. 2016 gives natural death rates of sheeps in Ndiagne, northern Senegal.
- Disease-induced mortality rate : In our model, infectious hosts were not separated between symptomatic and asymptomatic animals. Therefore, the disease-induced mortality rate could not be directly equal to the case fatality rate observed on clinical cases. Gaff et al. 2007 used values of 0.0176 and 0.0312, corresponding to case fatality rates of 15% and 25% respectively, with approximately 12% of symptomatic hosts in both populations.

Feeding preferences

Ba et al. (2006) did experiments with baited traps in the Ferlo region and provided monthly values of the percentage of mosquitoes found in each trap. They corrected the effect of host weight and CO_2 production by putting different numbers of animals in the trap depending on the species (1 veal, 2 sheeps). We computed weighted means from monthly values, because we did not consider preferences to vary over time. We normalized to account for cattle and small ruminants only, leaving aside other preys (Ba et al. 2006 also included human and chicken). Separate values for *Aedes vexans* and *C. poicilipes* were computed, the latter was also applied to *C. tritaeniorhynchus*. This species was also part of Ba et al. (2006) experiment but much less individuals were trapped so we favoured a bigger sample size for robustness.

2 Basic reproduction number

We used the next generation matrix method (van den Driessche and Watmough 2002) to determine the basic reproduction number R_0 of our ODE compartmental model. Let us sort our compartments so that the first m compartments correspond to infected individuals. We then expressed our system equations in the form $\frac{dx_i}{dt} = \mathcal{F}_i(x) - \mathcal{V}_i(x)$ for all compartments $x_i, 1 \leq i \leq m$ containing infected individuals. $\mathcal{F}_i(x)$ is the rate at which new infections arise and $\mathcal{V}_i(x)$ reflects vital dynamics, i.e the rate at which individuals enter or leave the compartment due to completion of an infection stage or death.

$$\frac{d}{dt}\begin{bmatrix} E_1 \\ I_1 \\ E_2 \\ I_2 \\ E_3 \\ I_3 \\ E_4 \\ I_4 \end{bmatrix} = \mathcal{F} - \mathcal{V} = \begin{bmatrix} a_1\phi_{12}\frac{I_2}{N_2}\alpha_{21}S_1 + a_1\phi_{13}\frac{I_3}{N_3}\alpha_{31}S_1 \\ 0 \\ a_1\phi_{12}\frac{I_1}{N_2}\alpha_{12}S_2 + a_4\phi_{42}\frac{I_4}{N_2}\alpha_{42}S_2 \\ 0 \\ a_1\phi_{13}\frac{I_1}{N_3}\alpha_{13}S_3 + a_4\phi_{43}\frac{I_4}{N_3}\alpha_{43}S_3 \\ 0 \\ a_4\phi_{42}\frac{I_2}{N_2}\alpha_{24}S_4 + a_4\phi_{43}\frac{I_3}{N_3}\alpha_{34}S_4 \\ 0 \end{bmatrix} - \begin{bmatrix} d_1E_1 + \epsilon_1E_1 \\ d_1I_1 - \epsilon_1E_1 \\ d_2E_2 + \epsilon_2E_2 \\ d_2I_2 + \gamma_2I_2 + \mu_2I_2 - \epsilon_2E_2 \\ d_3E_3 + \epsilon_3E_3 \\ d_3I_3 + \gamma_3I_3 + \mu_3I_3 - \epsilon_3E_3 \\ d_4I_4 + \epsilon_4E_4 \\ d_4I_4 - \epsilon_4E_4 \end{bmatrix}$$

We then defined the Jacobian matrices at disease-free equilibrium (DFE) x_0, $F = \left[\frac{\partial \mathcal{F}_i(x_0)}{\partial x_j}\right]$ and $V = \left[\frac{\partial \mathcal{V}_i(x_0)}{\partial x_j}\right], 1 \leq i, j \leq m$. Thus FV^{-1} is the next generation matrix K and $R_0 = \rho(K)$ where ρ denotes the spectral radius (largest eigenvalue).

Here, we considered the possibility for the DFE to incorporate a proportion of immune individuals. Thus, we had:

$S_i = N_i$ for vectors,$i \in \{1, 4\}$, and $S_j = (1 - p_j) \times N_j$ for hosts, $j \in \{2, 3\}$, p_j being the proportion of immune individuals among host population j.

$$F = \begin{pmatrix} 0 & 0 & 0 & a_1\phi_{12}\alpha_{21}\frac{N_1}{N_2} & 0 & a_1\phi_{13}\alpha_{31}\frac{N_1}{N_3} & 0 & 0 \\ 0 & 0 & 0 & 0 & 0 & 0 & & \\ 0 & a_1\phi_{12}\alpha_{12}(1-p_2) & 0 & 0 & 0 & 0 & 0 & a_4\phi_{42}\alpha_{42}(1-p_2) \\ 0 & 0 & 0 & 0 & 0 & 0 & 0 & 0 \\ 0 & a_1\phi_{13}\alpha_{13}(1-p_3) & 0 & 0 & 0 & 0 & 0 & a_4\phi_{43}\alpha_{43}(1-p_3) \\ 0 & 0 & 0 & 0 & 0 & 0 & 0 & 0 \\ 0 & 0 & 0 & a_4\phi_{42}\alpha_{24}\frac{N_4}{N_2} & 0 & a_4\phi_{43}\alpha_{34}\frac{N_4}{N_3} & 0 & 0 \\ 0 & 0 & 0 & 0 & 0 & 0 & 0 & 0 \end{pmatrix}$$

$$V = \begin{pmatrix} d_1+\epsilon_1 & 0 & 0 & 0 & 0 & 0 & 0 & 0 \\ -\epsilon_1 & d_1 & 0 & 0 & 0 & 0 & 0 & 0 \\ 0 & 0 & d_2+\epsilon_2 & 0 & 0 & 0 & 0 & 0 \\ 0 & 0 & -\epsilon_2 & d_2+\gamma_2+\mu_2 & 0 & 0 & 0 & 0 \\ 0 & 0 & 0 & 0 & d_3+\epsilon_3 & 0 & 0 & 0 \\ 0 & 0 & 0 & 0 & -\epsilon_3 & d_3+\gamma_3+\mu_3 & 0 & 0 \\ 0 & 0 & 0 & 0 & 0 & 0 & d_4+\epsilon_4 & 0 \\ 0 & 0 & 0 & 0 & 0 & 0 & -\epsilon_4 & d_4 \end{pmatrix}$$

$$K = F.V^{-1} = \begin{array}{c} \\ E_2 \\ E_3 \\ I_2 \\ I_3 \\ E_1 \\ E_4 \\ I_1 \\ I_4 \end{array} \begin{array}{c} \begin{array}{cccccccc} E_2 & E_3 & I_2 & I_3 & E_1 & E_4 & I_1 & I_4 \end{array} \\ \begin{pmatrix} 0 & 0 & 0 & 0 & k_{21} & k_{24} & \tilde{k_{21}} & \tilde{k_{24}} \\ 0 & 0 & 0 & 0 & k_{31} & k_{34} & \tilde{k_{31}} & \tilde{k_{34}} \\ 0 & 0 & 0 & 0 & 0 & 0 & 0 & 0 \\ 0 & 0 & 0 & 0 & 0 & 0 & 0 & 0 \\ k_{12} & k_{13} & \tilde{k_{12}} & \tilde{k_{13}} & 0 & 0 & 0 & 0 \\ k_{42} & k_{43} & \tilde{k_{42}} & \tilde{k_{43}} & 0 & 0 & 0 & 0 \\ 0 & 0 & 0 & 0 & 0 & 0 & 0 & 0 \\ 0 & 0 & 0 & 0 & 0 & 0 & 0 & 0 \end{pmatrix} \end{array}$$

Where k_{ij} is the number of cases in compartment i produced by an infectious individual from compartment j. $\tilde{k_{ij}}$ represent incomplete cycle of infections (I_j to E_i).

$K = \begin{pmatrix} 0 & A \\ B & 0 \end{pmatrix}$ with A representing vector-to-host transmission and B host-to-vector transmission. Therefore, AB and BA products represent 2 generations "like to like" transmission. Interestingly, R_0^2 is the dominant eigenvalue of both AB and BA (see Turner et al. 2013 Supporting Information for more details). We used the vector-to-host-to-vector generation matrix, which explains the presence of both vector populations in sub-parts of our R_0 and the sum to account for both host populations (see Eq 1-5 in main text). As a reminder, R_0 is a geometric mean, representing the average number of secondary cases arising from vector-to-host and host-to-vector transmission scenarios, as these were the only possible transmission routes in our system.

3 Removing outliers

Because we used a reservoir frequency-dependent transmission function (Wonham et al. 2006), we had to remove overestimation resulting from high vector-to-host ratios. We chose a threshold $\frac{N_1+N_4}{N_2+N_3} > 1000$.

Intro. date	Nb pixels contain hosts and vectors	Nb pixels removed due to ratio threshold	Nb pixels r0 computed
2014-07-07	2663	83	2580
2014-07-14	2667	85	2582
2014-07-21	2670	91	2579
2014-07-28	2679	111	2568
2014-08-04	2691	156	2535
2014-08-11	2710	170	2540
2014-08-18	2716	171	2545
2014-08-25	2717	143	2574
2014-09-01	2717	131	2586
2014-09-08	2717	154	2563
2014-09-15	2717	174	2543
2014-09-22	2717	185	2532
2014-09-29	2717	121	2596
2014-10-06	2717	75	2642
2014-10-13	2717	70	2647
2014-10-20	2717	68	2649
2014-10-27	2717	62	2655
2014-11-03	2717	62	2655
2014-11-10	2717	60	2657
2014-11-17	2717	109	2608
2014-11-24	2717	70	2647

Table S.1: **Pixel count for SRDV, 2014.** Number of pixels containing both hosts and vectors and number of pixels removed for having ($\frac{N_1+N_4}{N_2+N_3} > 1000$), giving the total number of pixels where R_0 is computed, for each introduction week.

Intro. date	Nb pixels contain hosts and vectors	Nb pixels removed due to ratio threshold	Nb pixels r0 computed
2015-07-13	2692	105	2587
2015-07-20	2710	134	2576
2015-07-27	2716	164	2552
2015-08-03	2717	177	2540
2015-08-10	2717	181	2536
2015-08-17	2717	169	2548
2015-08-24	2717	173	2544
2015-08-31	2717	197	2520
2015-09-07	2717	145	2572
2015-09-14	2717	194	2523
2015-09-21	2717	316	2401
2015-09-28	2717	135	2582
2015-10-05	2717	121	2596
2015-10-12	2717	133	2584
2015-10-19	2717	120	2597
2015-10-26	2717	101	2616
2015-11-02	2717	92	2625
2015-11-09	2717	89	2628
2015-11-16	2717	84	2633
2015-11-23	2717	76	2641
2015-11-30	2717	72	2645

Table S.2: **Pixel count for SRDV, 2015.** Number of pixels containing both hosts and vectors and number of pixels removed for having ($\frac{N_1+N_4}{N_2+N_3} > 1000$), giving the total number of pixels where R_0 is computed, for each introduction week.

Intro. date	Nb pixels contain hosts and vectors	Nb pixels removed due to ratio threshold	Nb pixels r0 computed
2016-07-11	2689	79	2610
2016-07-18	2702	130	2572
2016-07-25	2710	157	2553
2016-08-01	2717	178	2539
2016-08-08	2717	183	2534
2016-08-15	2717	171	2546
2016-08-22	2717	167	2550
2016-08-29	2717	180	2537
2016-09-05	2717	144	2573
2016-09-12	2717	152	2565
2016-09-19	2717	295	2422
2016-09-26	2717	143	2574
2016-10-03	2717	129	2588
2016-10-10	2717	124	2593
2016-10-17	2717	121	2596
2016-10-24	2717	106	2611
2016-10-31	2717	96	2621
2016-11-07	2717	89	2628
2016-11-14	2717	87	2630
2016-11-21	2717	75	2642
2016-11-28	2717	73	2644

Table S.3: **Pixel count for SRDV, 2016.** Number of pixels containing both hosts and vectors and number of pixels removed for having ($\frac{N_1+N_4}{N_2+N_3} > 1000$), giving the total number of pixels where R_0 is computed, for each introduction week.

Intro. date	Nb pixels contain hosts and vectors	Nb pixels removed due to ratio threshold	Nb pixels r0 computed
2014-07-07	1058	0	1058
2014-07-14	1102	0	1102
2014-07-21	1276	0	1276
2014-07-28	943	0	943
2014-08-04	890	0	890
2014-08-11	1035	0	1035
2014-08-18	1119	0	1119
2014-08-25	1285	0	1285
2014-09-01	1233	0	1233
2014-09-08	1132	0	1132
2014-09-15	1642	3	1639
2014-09-22	1680	7	1673
2014-09-29	1634	16	1618
2014-10-06	1550	18	1532
2014-10-13	1391	16	1375
2014-10-20	990	6	984
2014-10-27	720	2	718
2014-11-03	608	1	607
2014-11-10	502	1	501
2014-11-17	445	0	445
2014-11-24	54	0	54

Table S.4: **Pixel count for Ferlo, 2014.** Number of pixels containing both hosts and vectors and number of pixels removed for having ($\frac{N_1+N_4}{N_2+N_3} > 1000$), giving the total number of pixels where R_0 is computed, for each introduction week.

Intro. date	Nb pixels contain hosts and vectors	Nb pixels removed due to ratio threshold	Nb pixels r0 computed
2015-07-13	1140	0	1140
2015-07-20	1100	0	1100
2015-07-27	877	0	877
2015-08-03	1630	0	1630
2015-08-10	1632	0	1632
2015-08-17	1628	0	1628
2015-08-24	1702	0	1702
2015-08-31	1691	2	1689
2015-09-07	1603	9	1594
2015-09-14	1700	26	1674
2015-09-21	1695	48	1647
2015-09-28	1681	45	1636
2015-10-05	1702	41	1661
2015-10-12	1646	36	1610
2015-10-19	1305	29	1276
2015-10-26	846	18	828
2015-11-02	592	10	582
2015-11-09	498	2	496
2015-11-16	318	1	317
2015-11-23	60	0	60
2015-11-30	7	0	7

Table S.5: **Pixel count for Ferlo, 2015.** Number of pixels containing both hosts and vectors and number of pixels removed for having ($\frac{N_1+N_4}{N_2+N_3} > 1000$), giving the total number of pixels where R_0 is computed, for each introduction week.

Intro. date	Nb pixels contain hosts and vectors	Nb pixels removed due to ratio threshold	Nb pixels r0 computed
2016-07-11	973	0	973
2016-07-18	883	0	883
2016-07-25	674	0	674
2016-08-01	869	0	869
2016-08-08	1297	0	1297
2016-08-15	1267	0	1267
2016-08-22	1614	0	1614
2016-08-29	1407	1	1406
2016-09-05	1155	7	1148
2016-09-12	1172	16	1156
2016-09-19	1115	42	1073
2016-09-26	1006	46	960
2016-10-03	1185	41	1144
2016-10-10	968	38	930
2016-10-17	826	28	798
2016-10-24	700	19	681
2016-10-31	474	11	463
2016-11-07	325	3	322
2016-11-14	232	1	231
2016-11-21	76	0	76
2016-11-28	5	0	5

Table S.6: **Pixel count for Ferlo, 2016.** Number of pixels containing both hosts and vectors and number of pixels removed for having ($\frac{N_1+N_4}{N_2+N_3} > 1000$), giving the total number of pixels where R_0 is computed, for each introduction week.

4 Spatio-temporal pattern of R_0

	2014		2015		2016	
Region	**Ferlo**	**SRDV**	**Ferlo**	**SRDV**	**Ferlo**	**SRDV**
Nb pixels $R_0 > Q_{3,year}$	562	1588	436	2040	342	1996
mean nb events (weeks)	7.36	9.47	4.87	8.62	5.02	8.14
standard deviation nb events	3.37	5.06	2.99	5.02	2.89	4.83
	Total					
Nb pixels $R_0 > Q_{3,year}$	2150		2476		2338	
mean nb events (weeks)	8.92		7.96		7.71	
standard deviation nb events	4.77		4.93		4.73	

Table S.7: Detailed number of pixels reaching $R_0 > Q_{3,year}$, and the number of times it happens per pixel within the season, by study area. $Q_{3,year}$ is the third quartile of R_0 values, computed by season, independentely of the study area and date of virus introduction.

5 Insights for control programs

5.1 Relative vector abundances over the rainy season

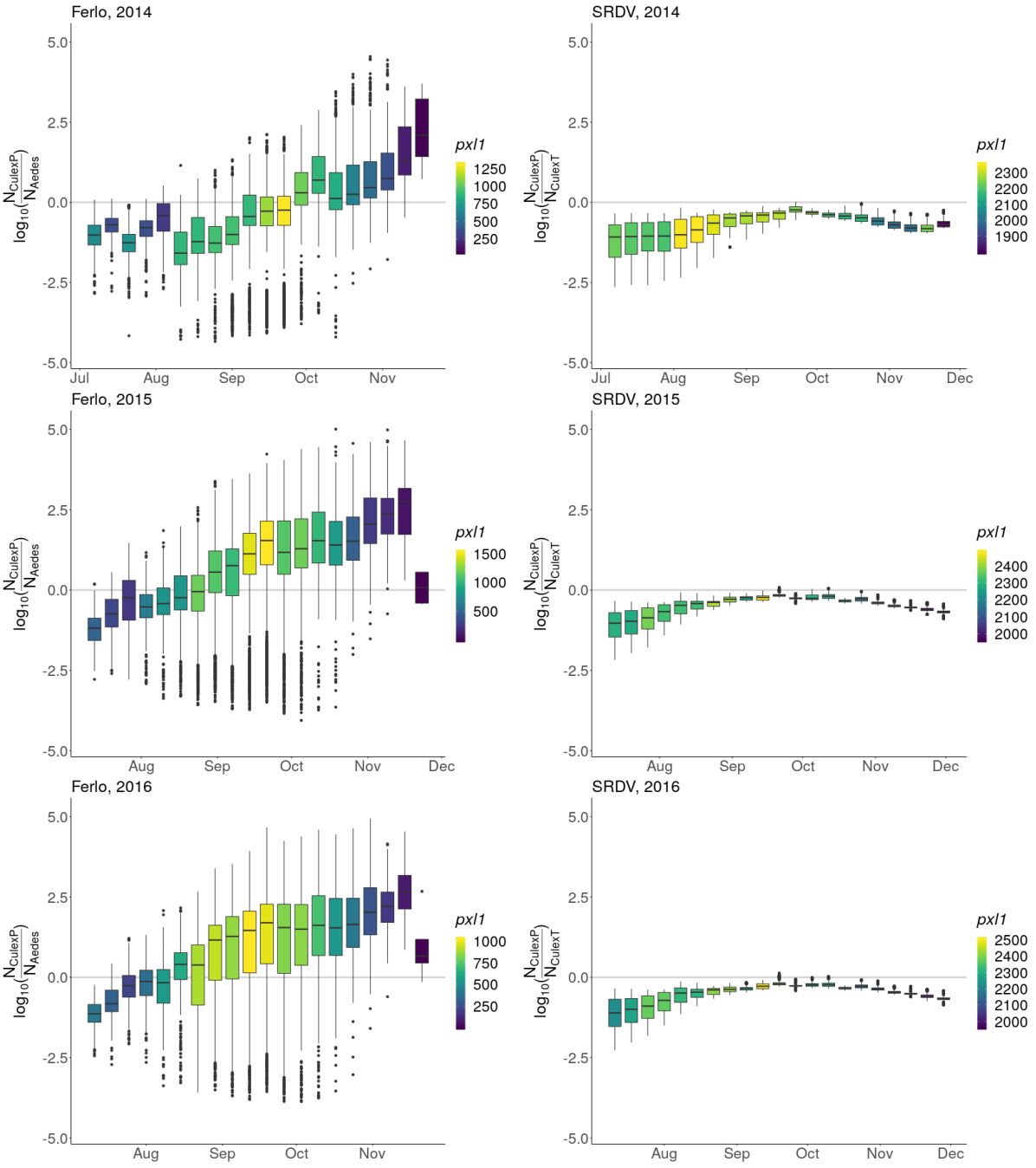

Figure S.4: Distribution of vector ratios ($log_{10}(\frac{N_{C.\ poicilipes}}{N_{Ae.\ v.\ arabiensis}})$ in the Ferlo, $log_{10}(\frac{N_{C.\ poicilipes}}{N_{C.\ tritaeniorhynchus}})$ in SRDV) among pixels of each study area having $R_0 > 1$, over the rainy seasons (from top to bottom, 2014 to 2016). Boxplots are coloured by the number of pixels with $R_0 > 1$ ($pxl1$) within the study area at each introduction date. In SRDV, the variability between pixels (range of the boxplots) is smaller than in the Ferlo, and *C. tritaeniorhynchus* is always more abundant than *C. poicilipes*. In the Ferlo, there is a time during each season where pixels with $R_0 > 1$ go from having on average more *Ae. v. arabiensis* than *C. poicilipes* to the opposite. This "switch" happens later in 2014 than in 2015 and 2016. The variability between pixels is important, for most virus introduction dates, there are pixels with both positive and negative $\log_{10}$ ratios among those with $R_0 > 1$.

5.2 Effect of herd immunity

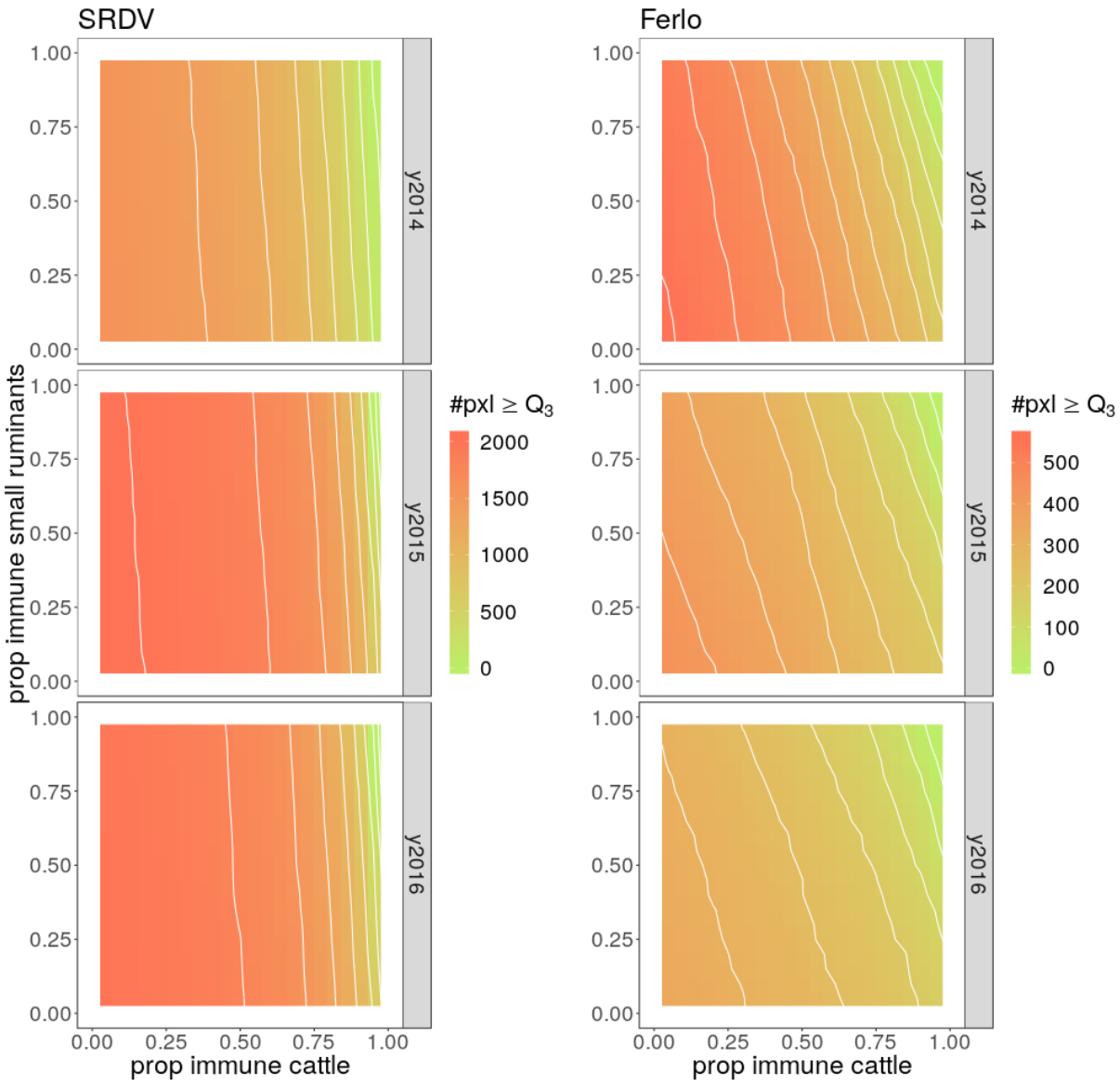

Figure S.5: Variation of the number of pixels with $R_0 > Q_{3,year}$ (third quartile of R_0 values) when increasing the immunity of the cattle population (x-axis) or small ruminant population (y-axis), by study area and season.

6 Sensitivity analysis

We performed a variance-based global sensitivity analysis using a Fourier Amplitude Sensitivity Testing (FAST, Saltelli et al. 2008). Parameters were varied within a 10% range using scaling factors (reference value of 1). A given set (scenario) of scaling factors was applied to all R_0 computations of a given study area and rainy season, to maintain the spatial heterogeneity as well as the relative temporal dynamics of vector densities and temperature-dependent parameters. Temperature-dependent function formulas were kept, and temperature was not varied. We sampled 10,000 values per parameter. We tested whether our results on introduction dates and locations with high epidemic potential were robust to these parameter variations.

6.1 Sensitivity of R_0 temporal pattern

	2014	2015	2016
SRDV	**08-11** (292,134) 08-04 (7,866)	09-14 (300,000)	09-12 (300,000)
Ferlo	09-22 (300,000)	**09-21** (299,999) 09-14 (1)	09-12 (300,000)

Table S.8: Introduction week inducing the highest number of pixels with $R_0 > 1$ for the different scenarios tested in the sensitivity analysis, by study area and rainy season. 30 parameters are varied within a 10% range, with 10,000 values sampled per parameter, which gives 300,000 scenarios. Number of scenarios giving the same introduction date is given in parenthesis. When two different dates are possible, the one given by the reference scenario is in bold.

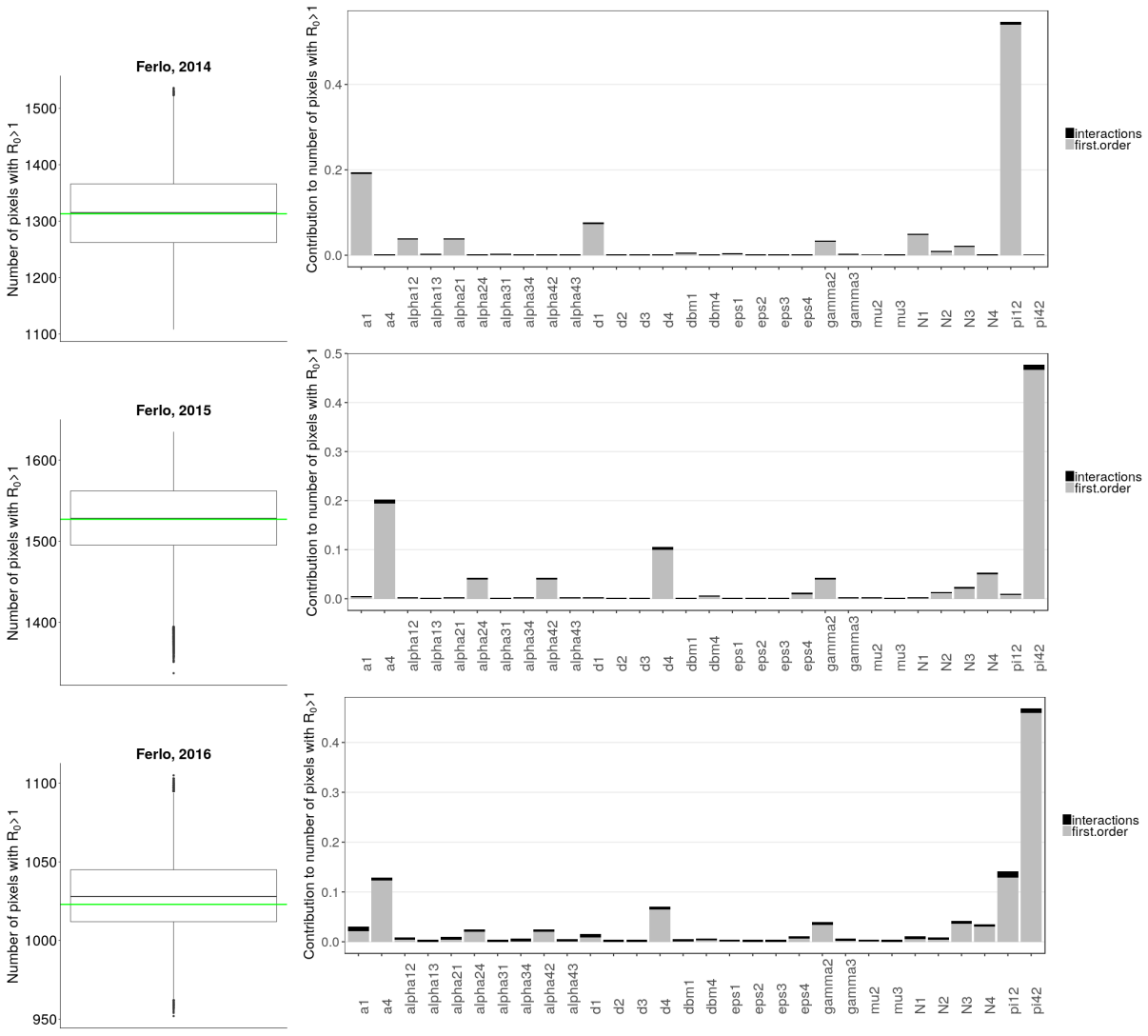

Figure S.6: Left : Distribution of $\max(pxl_1)_{year}$ among scenarios tested in the sensitivity analysis. Green line shows the value with reference parameters. In the box plots, the boundaries of the box indicate the 25^{th} (bottom) and 75^{th} (top) percentile. The line within the box marks the median. Whiskers above and below the box indicate the 10^{th} and 90^{th} percentiles. Points above and below the whiskers indicate outliers outside the 10^{th} and 90^{th} percentiles. Right : Contribution of model parameterers to pxl_1, for the introduction week inducing the highest pxl_1 of the rainy season. Results for the Ferlo, 2014 to 2016 (top to bottom).

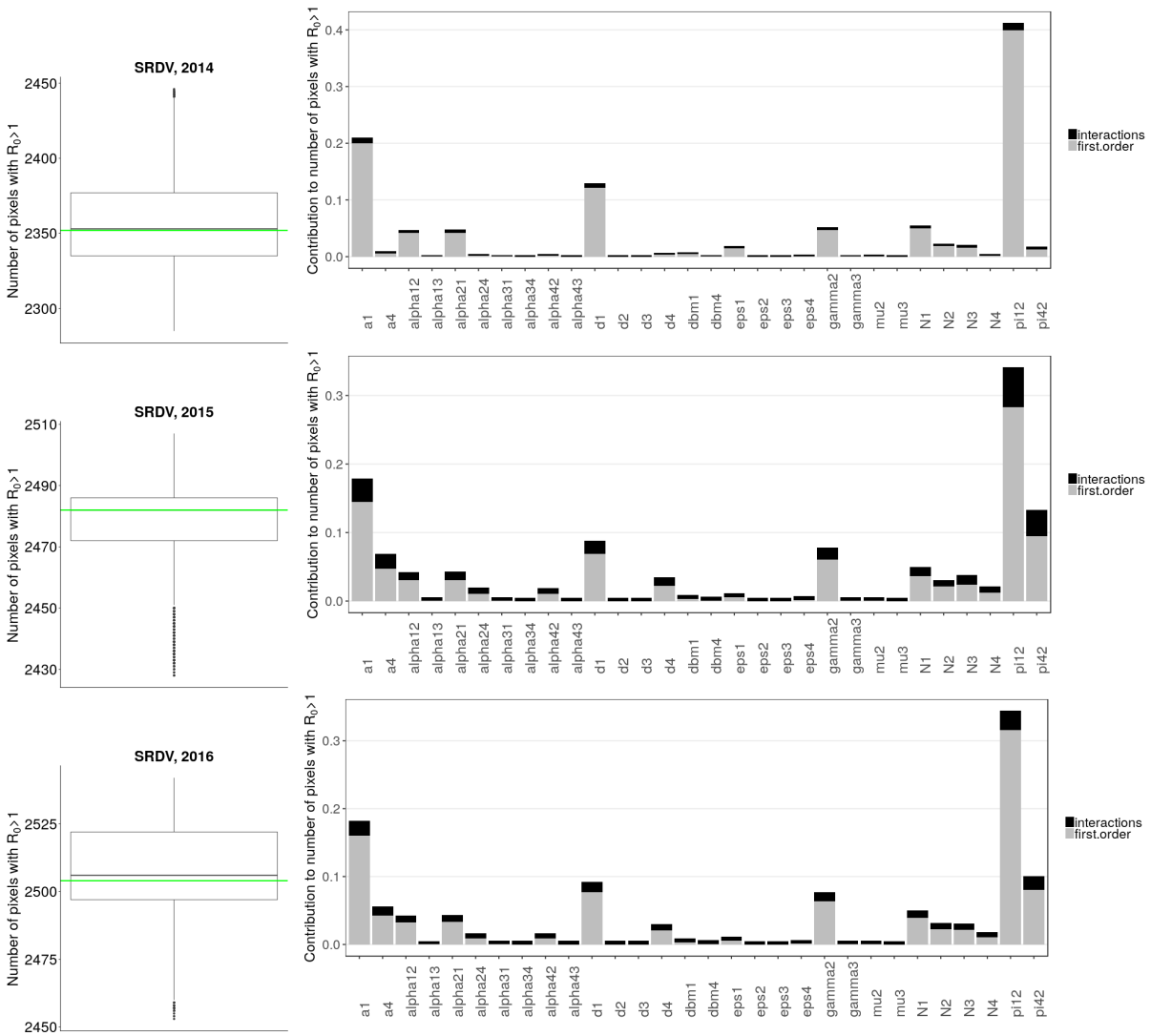

Figure S.7: Left : Distribution of $\max(pxl_1)_{year}$ among scenarios tested in the sensitivity analysis. Green line shows the value with reference parameters. In the box plots, the boundaries of the box indicate the 25^{th} (bottom) and 75^{th} (top) percentile. The line within the box marks the median. Whiskers above and below the box indicate the 10^{th} and 90^{th} percentiles. Points above and below the whiskers indicate outliers outside the 10^{th} and 90^{th} percentiles. Right : Contribution of model parameterers to pxl_1, for the introduction week inducing the highest pxl_1 of the rainy season. Results for SRDV, 2014 to 2016 (top to bottom).

6.2 Sensitivity of R_0 spatial pattern

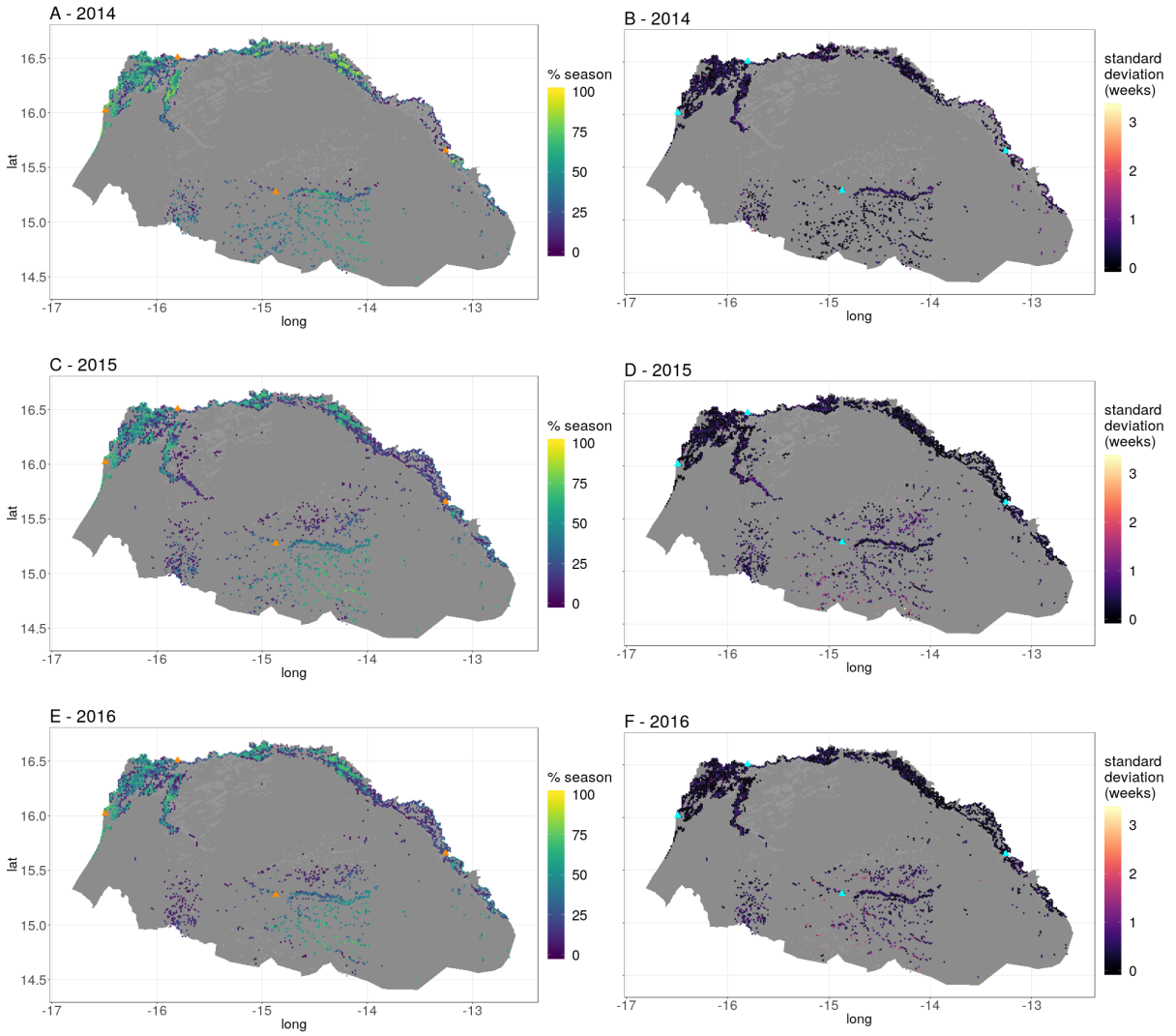

Figure S.8: Map of northern Senegal showing pixels with $R_0 \geq Q_{3,year}$ (third quartile of R_0 values) at least once in the season. Coloured pixels fill this criteria in at least one of the 300,000 scenarios tested in the sensitivity analysis, grey pixels do not. Left: Pixels are coloured by the average % of the season spent above the threshold (1 to 21 weeks) over all the scenarios. Right: Pixels are coloured by the standard deviation of the time spent above the threshold (1 to 21 weeks) over all the scenarios. Triangles are important locations to ease figure reading (left to right, top to bottom : Rosso, Saint-Louis, Matam, Barkedji).

7 References

Ba Y, Diallo D, Dia I, Diallo, M. Comportement trophique des vecteurs du virus de la fièvre de la vallée du Rift au Sénégal: implications dans l'épidémiologie de la maladie. Bull Soc Pathol Exot. 2006;7.

Barker CM, Niu T, Reisen WK, Hartley DM. Data-Driven Modeling to Assess Receptivity for Rift Valley Fever Virus. Turell MJ, editor. PLoS Neglected Tropical Diseases. 2013 Nov 14;7(11):e2515.

Crabtree MB, Kading RC, Mutebi J-P, Lutwama JJ, Miller BR. Identification of host blood from engorged mosquitoes collected in western Uganda using cytochrome oxidase I gene sequences. Journal of Wildlife Diseases. 2013 Jul;49(3):611–26.

van den Driessche P, Watmough J. Reproduction numbers and sub-threshold endemic equilibria for compartmental models of disease transmission. Mathematical Biosciences. 2002 Nov;180(1–2):29–48.

Edman JD, Downe AER. Host-blood sources and multiple-feeding habits of mosquitoes in Kansas. 1964;24(2):154-60.

Gaff HD, Hartley DM, Leahy NP. An epidemiological model of Rift Valley fever. 2007;12.

Gilbert M, Nicolas G, Cinardi G, Van Boeckel TP, Vanwambeke SO, Wint GRW, et al. Global distribution data for cattle, buffaloes, horses, sheep, goats, pigs, chickens and ducks in 2010. Scientific Data. 2018 Oct 30;5:180227.

Gordon SW, Tammariello RF, Linthicum KJ, Wirtz' RA, Digoutte JP. Feeding patterns of mosquitoes collected in the Senegal river basin. Journal of the american mosquito control association. 1991;7(3):424–32.

Hammami P, Lancelot R, Lesnoff M. Modelling the Dynamics of Post-Vaccination Immunity Rate in a Population of Sahelian Sheep after a Vaccination Campaign against Peste des Petits Ruminants Virus. Munderloh UG, editor. PLOS ONE. 2016 Sep 7;11(9):e0161769.

Madder DJ, Surgeoner GA, Helson BV. Number of Generations, Egg Production, and Developmental Time of Culex Pipiens and Culex Restuans (Diptera: Culicidae) in Southern Ontario1. Journal of Medical Entomology. 1983 May 26;20(3):275–87.

Muturi EJ, Muriu S, Shililu J, Mwangangi JM, Jacob BG, Mbogo C, et al. Blood-feeding patterns of Culex quinquefasciatus and other culicines and implications for disease transmission in Mwea rice scheme, Kenya. Parasitology Research. 2008 May;102(6):1329–35.

Ndiaye PI, Bicout DJ, Mondet B, Sabatier P. Rainfall triggered dynamics of Aedes mosquito aggressiveness. Journal of Theoretical Biology. 2006 Nov;243(2):222–9.

Saltelli, A, Chan, R, Scott, FM. Sensitivity analysis. Wiley. 2008. 494 p. ISBN: 978-0-470-74382-9.

Tran A, Fall AG, Biteye B, Ciss M, Gimonneau G, Castets M, et al. Spatial Modeling of Mosquito Vectors for Rift Valley Fever Virus in Northern Senegal: Integrating Satellite-Derived Meteorological Estimates in Population Dynamics Models. Remote Sensing. 2019 Apr 30;11(9):1024.

Turell MJ. Effect of environmental temperature on the vector competence of Aedes fowleri for rift valley fever virus. Research in Virology. 1989 Jan;140:147–54.

Turner J, Bowers RG, Baylis M. Two-Host, Two-Vector Basic Reproduction Ratio (R0) for Bluetongue. Gomez-Gardenes J, editor. PLoS ONE. 2013 Jan 8;8(1):e53128.

Wonham MJ, Lewis MA, Renclawowicz J, van den Driessche P. Transmission assumptions generate conflicting predictions in host-vector disease models: a case study in West Nile virus. Ecology Letters. 2006 Jun;9(6):706–25.

8 Credits

Regarding icons used in Figures 1, S.1, and the graphical abstract.
Droplets: made by Good Ware (https://www.flaticon.com/authors/good-ware), from Flaticon.
Sheep: made by Turkkub (https://www.flaticon.com/authors/turkkub), from Flaticon.
Temperature: made by Prosymbols (https://www.flaticon.com/authors/prosymbols), from Flaticon.
Cow: made by Freepik (https://www.flaticon.com/authors/freepik), from Flaticon.
Mosquito (Figures 1, S.1): made by Freepik, from Flaticon.
Mosquito (graphical abstract): made by Monkik (https://www.flaticon.com/authors/monkik), from Flaticon.